COMPARISON OF TWO NON-LINEAR SYSTEM IDENTIFICATION APPROACHES DERIVED FROM "REVERSE PATH" SPECTRAL ANALYSIS

C. M. RICHARDS

Analysis Tool Development Division, Caterpillar Inc., Peoria, IL 61614, U.S.A.

AND

R. SINGH

*Acoustics and Dynamics Laboratory, Department of Mechanical Engineering,
The Ohio State University, Columbus, OH 43210-1107, U.S.A.*

1. INTRODUCTION

For the identification of non-linear systems, new approaches have recently been formulated based upon the "reverse path" analysis [1–11]. Extensive application of the "reverse path" analysis for identifying single-degree-of-freedom (s.d.o.f.) systems has been demonstrated [1–8]. Others have extended the work for identification of multi-degree-of-freedom (m.d.o.f.) systems although differences in procedure exist [9–11]. For example, Rice and Fitzpatrick [11] use the "reverse path" analysis to formulate an identification process and their approach is illustrated by identifying a two-degree-of-freedom (d.o.f.) linear system with repeated natural frequencies and a two-d.o.f. non-linear system with cubic elastic forces. Richards and Singh [9] also utilize the "reverse path" analysis to formulate yet another procedure for identifying m.d.o.f. non-linear systems and apply the method to three- and five-d.o.f. systems with asymmetric and distributed non-linearities. To illustrate the essential similarities and differences that exist between these two methods, both procedures are formulated on a common basis and critically analyzed; and, a computational example is given illustrating the unique models identified by the two different identification methods. For the sake of brevity, the approach used by Rice and Fitzpatrick [11] will be referred to as Method A and the approach used by Richards and Singh [9] will be referred to as Method B.

2. INITIAL DERIVATION OF THE TWO APPROACHES

Identification of a mechanical or structural non-linear system from the "reverse path" analysis begins by measuring an applied random excitation $\mathbf{f}(t)$ and vibration response $\mathbf{x}(t)$. The measured data is then used to estimate a model to describe the physical system. The model originates from the generalized set of N coupled differential equations of motion

$$\hat{\mathbf{M}}\ddot{\mathbf{x}}(t) + \hat{\mathbf{C}}\dot{\mathbf{x}}(t) + \hat{\mathbf{K}}\mathbf{x}(t) + \mathbf{N}[\mathbf{x}(t), \dot{\mathbf{x}}(t)] = \mathbf{f}(t), \tag{1}$$

where $\hat{\mathbf{M}}$, $\hat{\mathbf{C}}$ and $\hat{\mathbf{K}}$ are estimated mass, viscous damping and stiffness matrices, respectively. Depending on the *a priori* knowledge of the locations and types of non-linearities present, the operator $\mathbf{N}[\mathbf{x}(t), \dot{\mathbf{x}}(t)]$ is composed of non-linear functions to best describe the restoring forces. If the locations of non-linearities and their respective forms are uncertain, additional functions may be included to capture the possible behavior of these unknown non-linearities. For example, it is feasible to assume non-linearities at all locations and attempt to describe these non-linearities by separate polynomial expansions. Successful identification will yield non-zero coefficients of significant terms in the expansion, and insignificant terms will have coefficients equal or close to zero. However, computation may become excessive and numerical conditioning problems may result. Therefore, any *a priori* knowledge of the locations and types of non-linearities should be employed to reduce the complexity of $\mathbf{N}[\mathbf{x}(t), \dot{\mathbf{x}}(t)]$, i.e., non-linear functions should only be included where non-linearities are likely to be located and these functions should contain terms with high probabilities of describing the nature of the non-linear restoring forces.

The Fourier transform $\mathscr{F}[\cdot]$ is applied to equation (1) to obtain a frequency domain model

$$\hat{\mathbf{B}}(\omega)\mathbf{X}(\omega) + \mathbf{\Gamma}(\omega) = \mathbf{F}(\omega),$$

$$\mathbf{X}(\omega) = \mathscr{F}[\mathbf{x}(t)], \qquad \mathbf{\Gamma}(\omega) = \mathscr{F}[\mathbf{N}[\mathbf{x}(t), \dot{\mathbf{x}}(t)]], \qquad \mathbf{F}(\omega) = \mathscr{F}[\mathbf{f}(t)], \quad (2\text{a–e})$$

$$\hat{\mathbf{B}}(\omega) = -\omega^2\hat{\mathbf{M}} + \mathrm{i}\omega\hat{\mathbf{C}} + \hat{\mathbf{K}},$$

where $\hat{\mathbf{B}}(\omega)$ is an estimate of the dynamic stiffness matrix. Beyond this initial system model described by the set of coupled non-linear frequency domain equations (2a), the final models identified by Methods A and B differ. Both methods essentially identify functions to describe the non-linear nature of the restoring forces. However, Method A identifies s.d.o.f. frequency response functions (FRFs) from which mass, damping and stiffness properties can be determined to represent the underlying linear system. Also excitations must be applied at each response location in order for the entire system to be identified. In contrast, Method B identifies FRFs in the m.d.o.f. system context. The m.d.o.f. parameter estimation techniques [12] are then employed to extract modal parameters of the underlying linear system. In addition, it is not necessary for excitations to be applied at every response location for full identification of the system.

3. METHOD A

In Method A, each equation of the N-dimensional model given by equation (2a) is considered individually:

$$\sum_{l=1}^{N}(-\omega^2\hat{m}_{pl} + \mathrm{i}\omega\hat{c}_{pl} + \hat{k}_{pl})X_l(\omega) + \sum_{j=1}^{n}\hat{a}_{pj}Y_{pj}(\omega) = F_p(\omega), \tag{3}$$

where p indicates the pth equation of the set of N equations (2a), and $\hat{m}_{pl}$, $\hat{c}_{pl}$ and $\hat{k}_{pl}$ are the estimated elements from the pth row and lth column of the mass matrix $\hat{\mathbf{M}}$, damping matrix $\hat{\mathbf{C}}$ and stiffness matrix $\hat{\mathbf{K}}$, respectively. The summation consists of n non-linear functions $y_{pj}(\mathbf{x}(t))$ chosen to describe the non-linear restoring forces acting on the pth d.o.f., where $Y_{pj}(\omega) = \mathscr{F}[y_{pj}(\mathbf{x}(t))]$ are the spectra of these functions and $\hat{a}_{pj}$ are their respective estimated coefficients. Note that $y_{pj}(\mathbf{x}(t))$ are known quantities calculated as a function of the

measured response $\mathbf{x}(t)$. For instance, assuming a cubic non-linear stiffness connecting m_1 and m_2 of some arbitrary system, then $y_{pj}(\mathbf{x}(t)) = (x_1(t) - x_2(t))^3$.

Although the next step does not effect the results, it is included in order to remain consistent with the formulation [11]. The non-linear functions $y_{pj}(\mathbf{x}(t))$ are multiplied out and terms of like form $z_{pj}(\mathbf{x}(t))$ are collected. Therefore,

$$\sum_{l=1}^{N} (-\omega^2 \hat{m}_{pl} + i\omega \hat{c}_{pl} + \hat{k}_{pl}) X_l(\omega) + \sum_{j=1}^{n'} \hat{b}_{pj} Z_{pj}(\omega) = F_p(\omega), \tag{4}$$

where $Z_{pj}(\omega) = \mathscr{F}[z_{pj}(\mathbf{x}(t))]$ and n' is the number of terms resulting from the expansion. As a result, $\hat{b}_{pj}$ are algebraic equations containing combinations of the coefficients $\hat{a}_{pj}$ of the original non-linear functions $y_{pj}(\mathbf{x}(t))$. Each of the N equations may be written in reverse form

$$F_p(\omega) = \sum_{l=1}^{N} (-\omega^2 \hat{m}_{pl} + i\omega \hat{c}_{pl} + \hat{k}_{pl}) X_l(\omega) + \sum_{j=1}^{n'} \hat{b}_{pj} Z_{pj}(\omega), \tag{5}$$

where $X_l(\omega)$ and $Z_{pj}(\omega)$ are scalar "inputs" to the pth equation and the measured excitation $F_p(\omega)$ at the pth response location is a scalar "output" of the equation. Equation (5) is illustrated in Figure 1 as a multiple-input/single-output (MISO) model. By applying proper spectral techniques [13], FRFs of each path of the model in Figure 1 can be identified. The FRFs correspond to the dynamic systems of order 0, 1 and 2. By inverting these identified FRFs, those corresponding to second order systems resemble s.d.o.f. FRFs from which $\hat{m}_{pl}$, $\hat{c}_{pl}$ and $\hat{k}_{pl}$ can be estimated using the s.d.o.f. modal analysis techniques [14]. From the FRFs corresponding to systems of order zero and one, the remaining $\hat{c}_{pl}$ and $\hat{k}_{pl}$ as well as the $\hat{b}_{pj}$ can be estimated by fitting curves of order zero and one to the spectrum. If desired, once all of the $\hat{m}_{pl}$, $\hat{c}_{pl}$ and $\hat{k}_{pl}$ for the pth model have been estimated, the linear damping an stiffness coefficients of the elastic and dissipative elements can be resolved from the equations of motion which must be explicitly known. Otherwise, $\hat{m}_{pl}$, $\hat{c}_{pl}$ and $\hat{k}_{pl}$ are used to construct $\hat{\mathbf{M}}$, $\hat{\mathbf{C}}$ and $\hat{\mathbf{K}}$. The coefficients $\hat{a}_{pj}$ of the original non-linear functions $Y_{pj}(\omega)$ can also be resolved from the algebraic equations $\hat{b}_{pj}$.
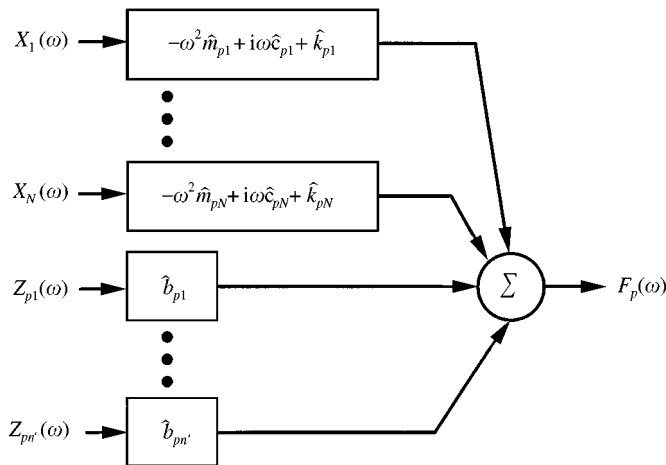
Figure 1. General MISO "reverse path" spectral model derived from Method A for the pth equation of motion, equation (5).

It should be strongly noted that this procedure can only be applied to the "reverse path" models given by equation (5) and illustrated in Figure 1, whose "inputs" $X_l(\omega)$ in particular are the responses of forced d.o.f.s. This is required in order for all of the "inputs" to the model to the uncorrelated. If this is not the case, then the responses of the unforced d.o.f.s can be described by a linear combination of the remaining "inputs". Consequently, erroneous estimates of the paths of the model may result. This concept is illustrate by an example in section 6.

4. METHOD B

Method B develops only one "reverse path" model from the entire set of N frequency domain equations of motion, i.e., equation (2a). These equations are written in reverse form as

$$\mathbf{F}(\omega) = \hat{\mathbf{B}}(\omega)\mathbf{X}(\omega) + \sum_{j=1}^{n} \hat{\mathbf{a}}_j \mathbf{Y}_j(\omega), \tag{6}$$

where $\mathbf{\Gamma}(\omega)$ has been replaced by the summation of spectra $\mathbf{Y}_j(\omega)$ of non-linear function vectors $\mathbf{y}_j(\mathbf{x}(t))$, i.e., $\mathbf{Y}_j(\omega) = \mathscr{F}[\mathbf{y}_j(\mathbf{x}(t))]$, multiplied by their corresponding coefficient matrices $\hat{\mathbf{a}}_j$ which are estimated from the identification process. The vectors $\mathbf{y}_j(\mathbf{x}(t))$ consist of non-linear functions of the same type, e.g., quadratic, cubic, fifth order, for describing the non-linear restoring forces and the elements of $\hat{\mathbf{a}}_j$ are the coefficients of these functions. Notice, $\mathbf{y}_j(\mathbf{x}(t))$ are known quantities calculated as a function of the measured response $\mathbf{x}(t)$. The vectors $\mathbf{Y}_j(\omega)$ are column vectors of length q_j, where q_j is the number of locations it is assumed that the jth type of non-linearity exists. The corresponding coefficient matrices $\hat{\mathbf{a}}_j$ are of dimension $N \times q_j$. It should be noted that formulation of the summation in equation (6) is not unique. For instance, one may wish to represent all of the non-linear functions by one single vector $\mathbf{Y}(\omega)$:

$$\sum_{j=1}^{n} \hat{\mathbf{a}}_j \mathbf{Y}_j(\omega) = \mathbf{A}\mathbf{Y}(\omega),$$

$$\mathbf{A} = [\hat{\mathbf{a}}_1 \ \hat{\mathbf{a}}_2 \ \cdots \ \hat{\mathbf{a}}_n], \qquad \mathbf{Y}(\omega) = [\mathbf{Y}_1(\omega)^{\mathrm{T}} \ \mathbf{Y}_2(\omega)^{\mathrm{T}} \ \cdots \ \mathbf{Y}_n(\omega)^{\mathrm{T}}]^{\mathrm{T}},$$

$$\tag{7}$$

where $\mathbf{Y}(\omega)$ is now a single vector containing all of the functions for describing the non-linear restoring forces and $\mathbf{A}$ contains all of the coefficients of these functions. However, the form of equation (6) was chosen so that the elements of $\hat{\mathbf{a}}_j$ have consistent units and for additional reasons discussed in reference [10]. Equation (6) is illustrated in Figure 2(a) as a "reverse path" system model. In contrast to Method A, here only one multi-input/multi-output (MIMO) model is formulated by keeping the system response and excitation in vector form, i.e., $\mathbf{X}(\omega) = [X_1(\omega) \ X_2(\omega) \ \cdots \ X_N(\omega)]^{\mathrm{T}}$, $\mathbf{F}(\omega) = [F_1(\omega) \ F_2(\omega) \ \cdots \ F_M(\omega)]^{\mathrm{T}}$, where M is the number of applied and measured excitations. Therefore, the path whose "input" is $\mathbf{X}(\omega)$ is the estimated dynamic stiffness matrix $\hat{\mathbf{B}}(\omega)$. By applying spectral conditioning techniques [9], an equivalent conditioned model is obtained. This model is illustrated in Figure 2(b) where the subscripts in parenthesis indicate that $\mathbf{Y}_{j(-1:j-1)}(\omega)$ contains the components of the spectra of the jth non-linear function vector $\mathbf{Y}_j(\omega)$ uncorrelated with the spectra $\mathbf{Y}_1(\omega)$ through $\mathbf{Y}_{j-1}(\omega)$ of the first through $j-1$ non-linear function vectors. See reference [9] for a more complete description of this process. The coefficient matrices $\hat{\mathbf{a}}_j$ have been transformed to $\hat{\mathbf{L}}_{jF}(\omega)$ due to the conditioning process. However, the $\hat{\mathbf{a}}_j$ can still be
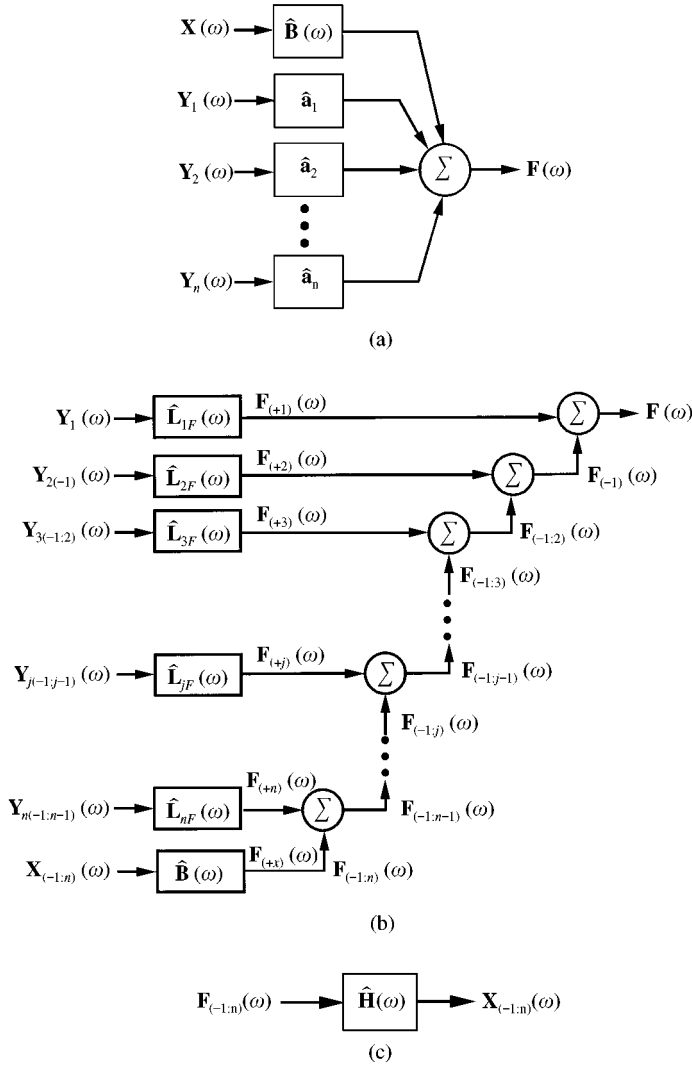
Figure 2. General MIMO "reverse path" spectral model derived from Method B. (a) Model with correlated inputs, equation (6). (b) Equivalent conditioned model with uncorrelated inputs. (c) "Forward path" of the underlying linear system.

recovered as discussed later. Notice that the last path of the conditioned model is the estimated dynamic stiffness matrix $\hat{\mathbf{B}}(\omega)$ uncharged by the conditioning process. Although the path itself remains uncharged, the "input" $\mathbf{X}_{(-1:n)}(\omega)$ of this path is now the conditioned system response vector which is uncorrelated with the n non-linear function vectors $\mathbf{Y}_1(\omega)$ through $\mathbf{Y}_n(\omega)$ as indicated by the subscript $(-1:n)$. This path alone can be re-reversed as shown in Figure 2(c) to identify m.d.o.f. dynamic compliance functions $\hat{\mathbf{H}}(\omega)$ using new conditioned frequency response estimates [9]:

$$\text{conditioned "}H_{c1}\text{" estimate: } [\hat{\mathbf{H}}^{[c1]}(\omega)]^{\mathrm{T}} = \mathbf{G}_{FF(-1:n)}^{-1}(\omega)\mathbf{G}_{FX(-1:n)}(\omega),$$

$$\text{(8a,b)}$$

$$\text{conditioned "}H_{c2}\text{" estimate: } [\hat{\mathbf{H}}^{[c2]}(\omega)]^{\mathrm{T}} = \mathbf{G}_{XF(-1:n)}^{-1}(\omega)\mathbf{G}_{XX(-1:n)}(\omega).$$

These estimates are the underlying linear dynamic compliance functions of the system and are unaffected by the non-linearities since $\mathbf{X}_{(-1:n)}(\omega)$ is uncorrelated with $\mathbf{Y}_1(\omega)$ through $\mathbf{Y}_n(\omega)$. Calculation of $\mathbf{G}_{XX(-1:n)}$, $\mathbf{G}_{XF(-1:n)}$ and $\mathbf{G}_{FF(-1:n)}$ is covered in reference [9]. Unlike Method A where s.d.o.f. techniques are used to extract physical properties from the s.d.o.f. FRFs, modal parameters of the underlying linear system are determined from the estimated m.d.o.f. dynamic compliance matrix $\hat{\mathbf{H}}(\omega)$ using the m.d.o.f. modal parameter identification methods [12]. Although not all of the elements $H_{ij}(\omega)$ of the matrix $\mathbf{H}(\omega)$ will be identified since excitations at all response locations are not required, reciprocity may be employed to obtain additional elements, i.e., $H_{ij}(\omega) = H_{ji}(\omega)$. This step allows for identification of non-linearities at locations away from applied excitations as discussed next and illustrated later by an example.

From the derivation given by the authors in reference [9], the coefficient matrices $\hat{\mathbf{a}}_j$ are estimated from the following recurrence equation:

$$\hat{\mathbf{a}}_j^T \hat{\mathbf{H}}^T(\omega) = \mathbf{G}_{jj(-1:j-1)}^{-1}(\omega)$$

$$\left(\mathbf{G}_{jF(-1:j-1)}(\omega)\hat{\mathbf{H}}^T(\omega) - \mathbf{G}_{jX(-1:j-1)}(\omega) - \sum_{i=j+1}^{n} \mathbf{G}_{ji(-1:j-1)}(\omega)\hat{\mathbf{a}}_i^T\hat{\mathbf{H}}^T(\omega) \right), \quad (9)$$

where one starts by solving for $\hat{\mathbf{a}}_n$ and ends solving for $\hat{\mathbf{a}}_1$. The left-hand side of equation (9) is multiplied out symbolically since not all of the elements of $\mathbf{H}(\omega)$ may be known if excitations are not applied at all response locations. In addition, estimation of some of the coefficients within the matrix $\hat{\mathbf{a}}_j$ may not be possible without use of additional elements of $\mathbf{H}(\omega)$. These additional elements can be determined by applying reciprocity, i.e., $H_{ij}(\omega) = H_{ji}(\omega)$. This procedure is more clearly illustrated by an example.

5. ILLUSTRATIVE EXAMPLE

To illustrate the two different approaches, consider the two-d.o.f. non-linear system of Figure 3(a). This is the same non-linear system used by Rice and Fitzpatrick [11] to illustrate their identification procedure where cubic non-linear spring elements exist between m_2 and m_1 and between m_1 are ground. Non-dimensional parameters are chosen identical to those used in reference [11]: $m_1 = 1\cdot0$, $m_2 = 0\cdot2$, $k_1 = 1\cdot0$, $k_c = 0\cdot2$, $c_1 = 0\cdot2$, $c_c = 0\cdot01$, $\beta_1 = 0\cdot05$, $\beta_c = 0\cdot05$. Initially, excitations are applied to both d.o.f.s. The case where only one excitation is applied ($f_1(t) = 0$) will also be considered. Excitations $f_1(t)$ and $f_2(t)$ are independent Gaussian excitations with $|f_1(t)| = |f_2(t)| = 5$ N-r.m.s., mean = 0 and variance = 1. To obtain the necessary input/output data for the identification process, a fifth order Runge–Kutta Fehlberg numerical integration algorithm is used [15]. The time steps (Δt) are held constant so that the fast Fourier transform (FFT) can be applied to the data, and high-frequency numerical simulation errors are minimized by choosing a Nyquist frequency 16 times greater than the highest frequency of interest. The following numerical simulation parameters are used: $\Delta t = 62\cdot5$ ms, number of samples $= 15(2^{14})$, total period $= 15(2^{10})$ ms. Note, results presented here will be different than that reported in reference [11] since numerical simulation and signal processing parameters are different.

Before the application of the non-linear system identification techniques, linear identification is employed to illustrate the effects that the non-linear spring elements have on the response of the system. Figure 3(b) illustrates the magnitude of a frequency response function $\hat{H}_{12}^{[1]}(\omega)$ estimated using the conventional "H_1" estimation method [16], where superscript [1] indicates an "H_1" estimate and the subscripts indicate that this is a cross-function between the response $X_1(\omega)$ and excitation $F_2(\omega)$. The following procedure
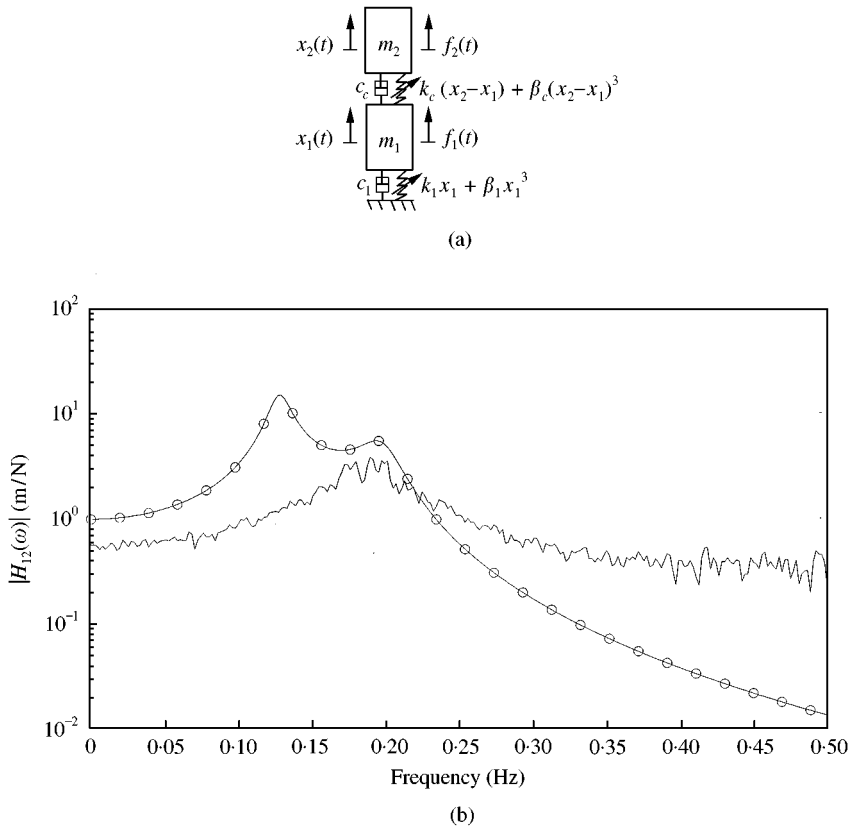
Figure 3. Two d.o.f. example system. (a) Physical system with cubic non-linear spring elements (b) Magnitude of dynamic compliance spectra $H_{12}(\omega)$: ——, $|\hat{H}_{12}^{[1]}(\omega)|$; –O–O–, $|H_{12}(\omega)|$.

is used for all spectral calculations presented throughout this article. The sampled data are first divided into 30 averages consisting of 2^{13} samples per average. Since the Nyquist frequency is much greater than the highest frequency of interest, an eighth order Chebyshev type-I low-pass filter with a cut-off frequency at 0.5 Hz is applied next. The data are then re-sampled at a new $\Delta t' = 16\Delta t$ and a Hanning window is employed to remove leakage errors. Also shown is the corresponding dynamic compliance function $H_{12}(\omega)$ of the underlying linear system synthesized from the systems linear parameters, i.e., mass, damping and linear stiffness matrices. This compliance function would result if the non-linearities did not exist, i.e., $\beta_1 = \beta_2 = 0$ or if the excitation was low such that the non-linear elastic force terms had no detectable effects. However, since excitation was chosen high enough to produce significant non-linear response, estimated compliance functions such as $\hat{H}_{12}^{[1]}(\omega)$ in Figure 3(b) result. As illustrated, the estimated compliance function is highly corrupted by the effects of the non-linear spring elements and the use of m.d.o.f. modal parameter estimation techniques for extracting effective modal parameters for this excitation level would be ineffective and hence no model could be developed. To overcome this obstacle, methods for the identification of non-linear systems such as those discussed in this paper are applied.

For the non-linear system identification techniques, Methods A and B, the assumption is made that the location and types of non-linearities are known, i.e., cubic non-linear stiffness elements exist at both junctions of the example system. However, as mentioned in section 2,

this assumption is not required for the application of either of the two methods. The system model is based on the equations of motion given here in both time and frequency domains:

$$\hat{\mathbf{M}}\ddot{\mathbf{x}}(t) + \hat{\mathbf{C}}\dot{\mathbf{x}}(t) + \hat{\mathbf{K}}\mathbf{x}(t) + \hat{\mathbf{a}}_1\,\mathbf{y}_1(t) = \mathbf{f}(t),$$

$$\hat{\mathbf{M}} = \begin{bmatrix} \hat{m}_1 & 0 \\ 0 & \hat{m}_2 \end{bmatrix}, \quad \hat{\mathbf{C}} = \begin{bmatrix} \hat{c}_1 + \hat{c}_c & -\hat{c}_c \\ -\hat{c}_c & \hat{c}_c \end{bmatrix}, \quad \hat{\mathbf{K}} = \begin{bmatrix} \hat{k}_1 + \hat{k}_c & -\hat{k}_c \\ -\hat{k}_c & \hat{k}_c \end{bmatrix}, \quad \hat{\mathbf{a}}_1 = \begin{bmatrix} \hat{\beta}_1 & -\hat{\beta}_c \\ 0 & \hat{\beta}_c \end{bmatrix},$$

$$\mathbf{x}(t) = \begin{Bmatrix} x_1(t) \\ x_2(t) \end{Bmatrix}, \qquad \mathbf{y}_1(t) = \begin{Bmatrix} x_1(t)^3 \\ (x_2(t) - x_1(t))^3 \end{Bmatrix}, \qquad \mathbf{f}(t) = \begin{Bmatrix} f_1(t) \\ f_2(t) \end{Bmatrix},$$

$$\text{(10a, b)}$$

$$\hat{\mathbf{B}}(\omega)\mathbf{X}(\omega) + \hat{\mathbf{a}}_1\mathbf{Y}_1(\omega) = \mathbf{F}(\omega),$$

$$\hat{\mathbf{B}} = \begin{bmatrix} \hat{B}_{11}(\omega) & \hat{B}_{12}(\omega) \\ \hat{B}_{21}(\omega) & \hat{B}_{22}(\omega) \end{bmatrix}, \qquad \mathbf{X}(\omega) = \mathscr{F}[\mathbf{x}(t)], \qquad \mathbf{F}(\omega) = \mathscr{F}[\mathbf{f}(t)],$$

$$\mathbf{Y}_1(\omega) = \mathscr{F}[\mathbf{y}_1(t)] = \mathscr{F}\left[\begin{Bmatrix} x_1(t)^3 \\ (x_2(t) - x_1(t))^3 \end{Bmatrix} \right] = \begin{Bmatrix} \mathscr{F}[x_1(t)^3] \\ \mathscr{F}[(x_2(t) - x_1(t))^3] \end{Bmatrix} = \begin{Bmatrix} Y_1(\omega) \\ Y_2(\omega) \end{Bmatrix},$$

where $\hat{B}_{qk}(\omega) = -\omega^2\hat{M}_{qk} + i\omega\hat{C}_{qk} + \hat{K}_{qk}$ and $\hat{M}_{qk}$, $\hat{C}_{qk}$ and $\hat{K}_{qk}$ are the elements of the qth row and kth column of the matrices $\hat{\mathbf{M}}$, $\hat{\mathbf{C}}$ and $\hat{\mathbf{K}}$, respectively. As previously shown in the analytical development, the two identification approaches deviate in methodology from this point onwards.

6. APPLICATION OF METHOD A

For Method A, each equation of the frequency domain system of equations (10b), is identified separately using the "reverse path" analysis:

$$F_1(\omega) = \hat{B}_{11}(\omega)X_1(\omega) + \hat{B}_{12}(\omega)X_2(\omega) + \hat{\beta}_1 Y_1(\omega) - \hat{\beta}_c Y_2(\omega),$$

$$\text{(11a, b)}$$

$$F_2(\omega) = \hat{B}_{21}(\omega)X_1(\omega) + \hat{B}_{22}(\omega)X_2(\omega) + \hat{\beta}_c Y_2(\omega).$$

To remain consistent with the formulation of Rice and Fitzpatrick [11], the non-linear function $Y_2(\omega)$ is expanded, $Y_2(\omega) = \mathscr{F}[(x_2(t) - x_1(t))^3] = Z_1(\omega) - 3Z_2(\omega) + 3Z_3(\omega) - Z_4(\omega)$, where $Z_1(\omega) = \mathscr{F}[x_2(t)^3]$, $Z_2(\omega) = \mathscr{F}[x_2(t)^2 x_1(t)]$, $Z_3(\omega) = \mathscr{F}[x_2(t)x_1(t)^2]$, $Z_4(\omega) = \mathscr{F}[x_1(t)^3]$. Therefore,

$$F_1(\omega) = \hat{B}_{11}(\omega)X_1(\omega) + \hat{B}_{12}(\omega)X_2(\omega) - \hat{\beta}_c Z_1(\omega) + 3\hat{\beta}_c Z_2(\omega) + 3\hat{\beta}_c Z_3(\omega) + (\hat{\beta}_1 + \hat{\beta}_c)Z_4(\omega),$$

$$\text{(12a, b)}$$

$$F_2(\omega) = \hat{B}_{21}(\omega)X_1(\omega) + \hat{B}_{22}(\omega)X_2(\omega) + \hat{\beta}_c Z_1(\omega) - 3\hat{\beta}_c Z_2(\omega) + 3\hat{\beta}_c Z_3(\omega) - \hat{\beta}_c Z_4(\omega)$$

Equations (12a, b) are illustrated in Figure 4(a, b) as two MISO models. Identification of these models commences using conventional techniques for MISO systems [13]. Beginning with the identification of the model in Figure 4(a) results in spectra for each of the six paths of the model. As discussed in the derivation, the inverse of these spectra are analyzed. Therefore, the spectrum corresponding to $\hat{B}_{11}(\omega) = -\omega^2\hat{M}_{11} + i\omega\hat{C}_{11} + \hat{K}_{11} = -\omega^2\hat{m}_1 + i\omega(\hat{c}_1 + \hat{c}_c) + (\hat{k}_1 + \hat{k}_c)$ is graphed as $|1/\hat{B}_{11}(\omega)|$ in Figure 5(a). As a result, this spectrum resembles that of a s.d.o.f. mechanical oscillator. Also plotted in Figure 5(a) is the inverse of
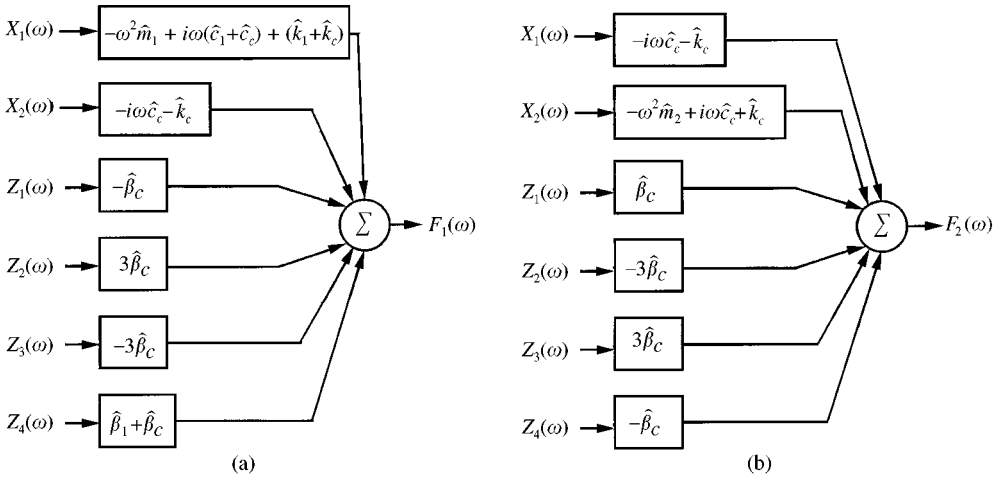
Figure 4. MISO "reverse path" spectral models of example system derived from Method A. (a) First equation of motion, equation 12(a). (b) Second equation of motion, equation 12(b).

the corresponding dynamic stiffness function $B_{11}(\omega)$ of the underlying linear system that was synthesized using the systems mass, damping and linear stiffness coefficients. As with the synthesized compliance function $H_{12}(\omega)$ illustrated in Figure 3(b), this dynamic stiffness function would result if the non-linearities did not exist. By applying linear s.d.o.f. identification techniques [14], $\hat{m}_1$, $(\hat{c}_1 + \hat{c}_c)$ and $(\hat{k}_1 + \hat{k}_c)$ can be determined from the spectrum $1/\hat{B}_{11}(\omega)$. Since $1/\hat{B}_{11}(\omega)$ is an accurate estimate of the synthesized dynamic stiffness function of the underlying linear system, $\hat{m}_1$, $(\hat{c}_1 + \hat{c}_c)$ and $(\hat{k}_1 + \hat{k}_c)$ will be accurate estimates of the actual m_1, $(c_1 + c_c)$ and $(k_1 + k_c)$.

The spectrum of the first order system $\hat{B}_{12}(\omega) = -\omega^2 \hat{M}_{12} + i\omega \hat{C}_{12} + \hat{K}_{12} = -i\omega \hat{c}_c - \hat{k}_c$ is graphed in Figure 5(b, c) as $\mathrm{Re}[\hat{B}_{12}(\omega)]$ and $\mathrm{Im}[\hat{B}_{12}(\omega)]$, where $\mathrm{Re}[\cdot]$ indicates real part and $\mathrm{Im}[\cdot]$ indicates imaginary part of $\hat{B}_{12}(\omega)$. Since $\mathrm{Re}[\hat{B}_{12}(\omega)] = \mathrm{Re}[-i\omega \hat{c}_c - \hat{k}_c] = -\hat{k}_c$ and $\mathrm{Im}[\hat{B}_{12}(\omega)] = \mathrm{Im}[-i\omega \hat{c}_c - \hat{k}_c] = -\omega \hat{c}_c$, the spectrum $\mathrm{Re}[\hat{B}_{12}(\omega)]$ is spectrally independent and approximately equal to $-k_c$. Likewise, the spectrum $\mathrm{Im}[\hat{B}_{12}(\omega)]$ is equal to zeros at $\omega = 0$ with slope of $-c_c$. Note, $\hat{B}_{12}(\omega)$ has been illustrated somewhat differently here compared with how $\hat{B}_{12}(\omega)$ was illustrated in reference [11]. Although this has no impact on the estimated quantities, the authors found it easier to determine the quantities k_c and c_c by illustrating $\hat{B}_{12}(\omega)$ as $\mathrm{Re}[\hat{B}_{12}(\omega)]$ and $\mathrm{Im}[\hat{B}_{12}(\omega)]$.

For the identification of the third path, since $-\beta_c$ is a real constant, the spectrum of $-\hat{\beta}_c$ should be independent of frequency and real-valued approximately equal to $-\beta_c$. The real part of this spectrum is shown in Figure 5(d). As shown, $\mathrm{Re}[-\hat{\beta}_c]$ is a good approximation of $-\beta_c$. Although not illustrated, the imaginary part of the spectrum is approximately zero. The identified spectra of the fourth and fifth paths are not shown since they are ratios of the third path. The spectrum of the sixth path, i.e., $(\hat{\beta}_1 + \hat{\beta}_c)$, is also not shown. However, the real part of the spectrum is approximately equal to $\beta_1 + \beta_c$ and the imaginary part is approximately zero. Therefore, an accurate estimate has resulted. Since $\hat{\beta}_c$ was determined from the spectrum of the third path, $\hat{\beta}_1$ can be determined from the spectrum of the sixth path.

Proceeding to the identification of the model in Figure 4(b) results in spectra for each of the six paths of this model. The spectra are not illustrated here, however the accuracy of the results are similar to the accuracy of the results shown for the model in Figure 4(a). By
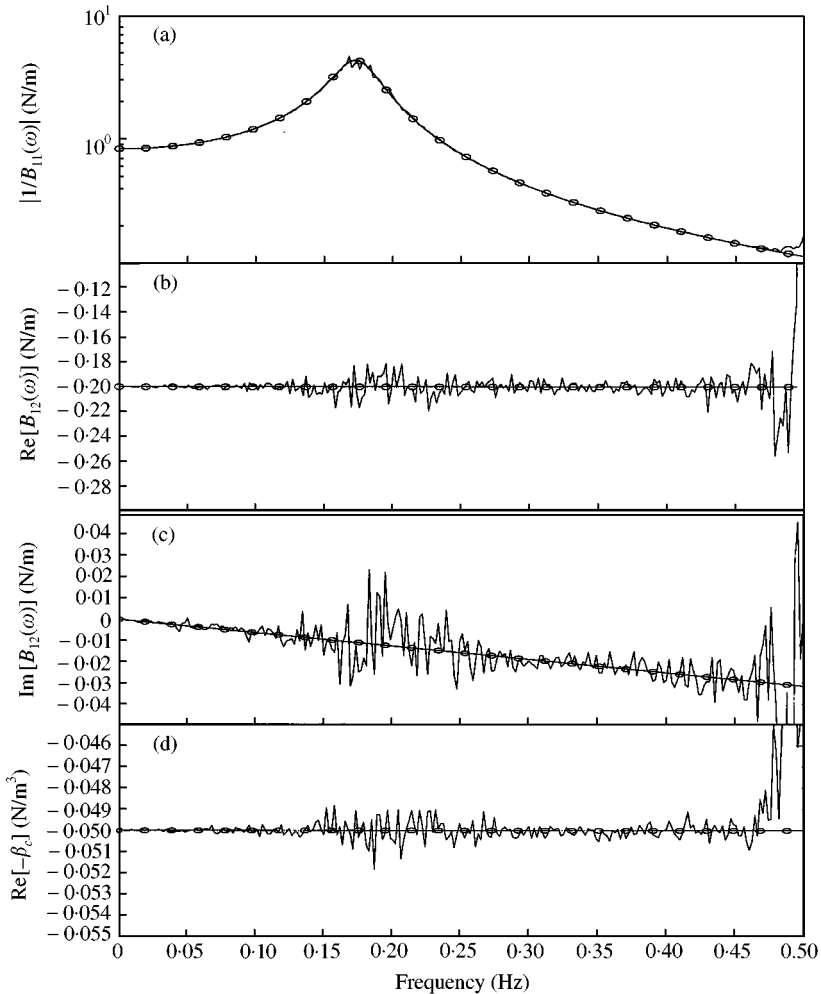
Figure 5. Multi-excitation results of Method A. (a) Magnitude of inverse spectrum of second order system $B_{11}(\omega)$: ——, $|1/\hat{B}_{11}(\omega)|$; –O–O–, $|1/B_{11}(\omega)|$. (b) Real part of first order system $B_{12}(\omega)$: ——, $\mathrm{Re}\,[\hat{B}_{12}(\omega)]$; –O–O–, $-k_c$. (c) Imaginary part of first order system $B_{12}(\omega)$: ——, $\mathrm{Im}\,[\hat{B}_{12}(\omega)]$; –O–O–, $-\omega c_c$. (d) Real part of spectral estimate of coefficient β_c: ——, $\mathrm{Re}\,[-\hat{\beta}_c]$; –O–O–, $-\beta_c$.

applying linear s.d.o.f. identification techniques [14] to the spectrum of $1/\hat{B}_{22}(\omega)$, $\hat{m}_2$, $\hat{c}_c$ and $\hat{k}_c$ can be estimated.

With excitation applied to both m_1 and m_2 of the example system, a fully identified model has been determined using Method A. However, identification of the example system will now be conducted using Method A with only one excitation applied to m_2. The example system is again simulated to calculate response data using the same simulation parameters described in section 5 with the exception that $f_1(t) = 0$. The identification process is carried through as before, however the "output" of the model illustrated in Figure 4(a) is zero; or in other words, the left-hand side of equation 12(a) is zero. Therefore, the identification process proceeds with the identification of the model illustrated in Figure 4(b). Estimated spectra of the first two paths of the model, $\hat{B}_{22}(\omega)$ and $\hat{B}_{21}(\omega)$, are shown in Figure 6(a, b). As illustrated, these spectra are inaccurate estimates of $B_{22}(\omega)$ and $B_{21}(\omega)$. This result is due to the dependence between the "inputs" to the "reverse path" model. Since no independent
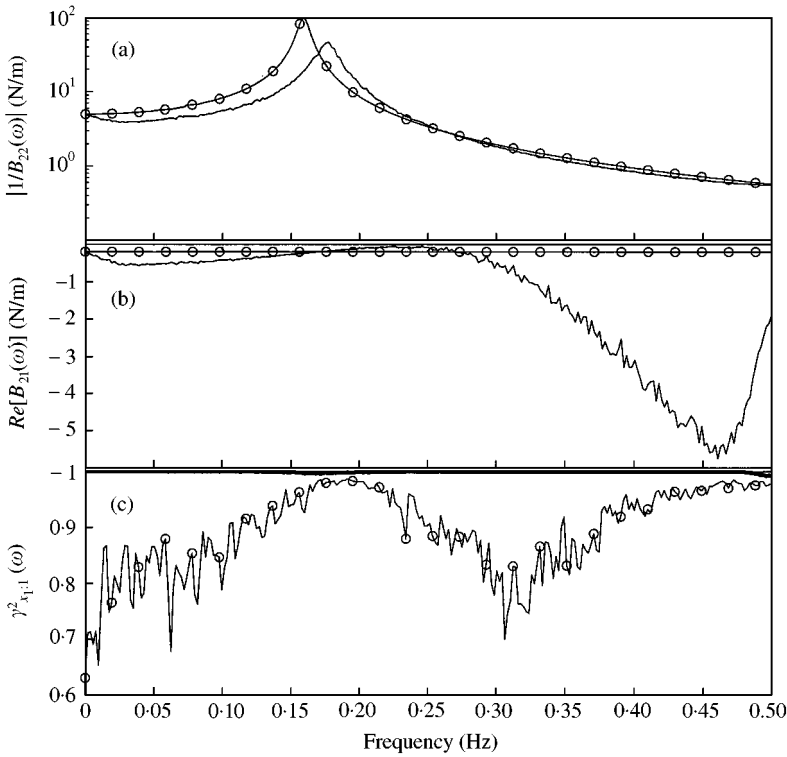
Figure 6. Single excitation results of Method A. (a) Magnitude of inverse spectrum of second order system $B_{22}(\omega)$: ——, $|1/\hat{B}_{22}(\omega)|$; –O–O–, $|1/B_{22}(\omega)|$. (b) Real part of first order system $B_{21}(\omega)$: ——, Re$[\hat{B}_{21}(\omega)]$; –O–O–, $-k_c$. (c) Multiple coherence $\gamma^2_{X_1:I}(\omega)$: ——, single excitation case; –O–O–, multi-excitation case.

random excitation is applied to m_1, the response $X_1(\omega)$ can be described by linear combinations of the remaining "inputs" to the model, i.e., $X_2(\omega)$ and $Z_1(\omega)$ through $Z_4(\omega)$. This linear dependence can be proved by the multiple coherence function $\gamma^2_{X_1:I}(\omega)$ between $X_1(\omega)$ and the remaining "inputs" $I \in [X_2(\omega), Z_1(\omega), Z_2(\omega), Z_3(\omega), Z_4(\omega)]$. The significance of $\gamma^2_{X_1:I}(\omega)$ is that a value of 1 for a given value of ω indicates that $X_1(\omega)$ can be obtained by linear operations of the other "inputs" [13]. A plot of $\gamma^2_{X_1:I}(\omega)$ is shown in Figure 6(c) for the single excitation case considered here, and also for the previously investigated multi-excitation case. Notice that for the single excitation case, $\gamma^2_{X_1:I}(\omega)$ is unity over the entire frequency range ($0 \leqslant \omega \leqslant \pi$) indicating that $X_1(\omega)$ is not providing any unique information to the "output" of the model. Consequently, the model in Figure 4(b) is poorly defined for the single-excitation case and poor estimates of all of the model's paths result. This is in contrast to the previously investigated multi-excitation case where $\gamma^2_{X_1:I}(\omega)$ does not attain unity for any value of ω($0 \leqslant \omega \leqslant \pi$), Here $\gamma^2_{X_1:I}(\omega)$ indicates that $X_1(\omega)$ cannot be obtained by a linear combination of the other "inputs" to the model ($X_2(\omega)$, $Z_1(\omega)$ through $Z_4(\omega)$) due to the independently applied excitation $F_1(\omega)$. As a result, the estimated spectra are accurate as was previously shown.

It should be noted that although Method A was unsuccessful at accurately identifying the example system with one excitation, the method can still be applied to systems that do not have excitations applied at every response location. However, only the "reverse path" models for the system given by equation (5) and illustrated in Figure 1 whose "inputs" $X_l(\omega)$ are responses of forced d.o.f.s will be accurately identified. This corresponds only to forced

d.o.f.s that are coupled only to forced d.o.f.s. Any of the "reverse path" models whose "inputs" $X_I(\omega)$ are responses of unforced d.o.f.s should not yield accurate spectrum of the models paths, as the example has illustrated. Therefore, not all of the system can be accurately identified unless excitations are applied at every response location.

7. APPLICATION OF METHOD B

Specific application of the authors' approach to the example system is as follows. First consider the case with excitations applied to both d.o.f.s. The system of equations 10(b) as a whole are written in reverse form as one m.d.o.f. model:

$$\begin{Bmatrix} F_1(\omega) \\ F_2(\omega) \end{Bmatrix} = \begin{bmatrix} \hat{B}_{11}(\omega) & \hat{B}_{12}(\omega) \\ \hat{B}_{21}(\omega) & \hat{B}_{22}(\omega) \end{bmatrix} \begin{Bmatrix} X_1(\omega) \\ X_2(\omega) \end{Bmatrix} + \begin{bmatrix} \hat{\beta}_1 & -\hat{\beta}_c \\ 0 & \hat{\beta}_c \end{bmatrix} \begin{Bmatrix} Y_1(\omega) \\ Y_2(\omega) \end{Bmatrix}. \tag{13}$$

The MIMO model is illustrated in Figure 7(a). Note that the "inputs" and "outputs" are in vector form and the path corresponding to the vector "input" $\mathbf{X}(\omega)$ is the dynamic stiffness matrix $\hat{\mathbf{B}}(\omega)$. Spectral conditioning [9] is applied to the "inputs" and "outputs" of this model to obtain an equivalent conditioned model as illustrated in Figure 7(b). The second path of the conditioned system is re-reversed as shown in Figure 7(c) and dynamic compliance functions are estimated, with influences from the non-linearities removed, using one of the conditioned frequency response estimators of equations 8(a, b). One of the estimated dynamic compliance functions $\hat{H}_{22}^{[c2]}(\omega)$ is illustrated in Figure 8(a), where superscript $[c2]$ indicates a conditioned "H_{c2}" estimate calculated by equation 8(b). Also plotted is the corresponding underlying linear system's dynamic compliance function synthesized from $\mathbf{M}$, $\mathbf{C}$ and $\mathbf{K}$ as discussed in section 5. Using m.d.o.f modal parameter
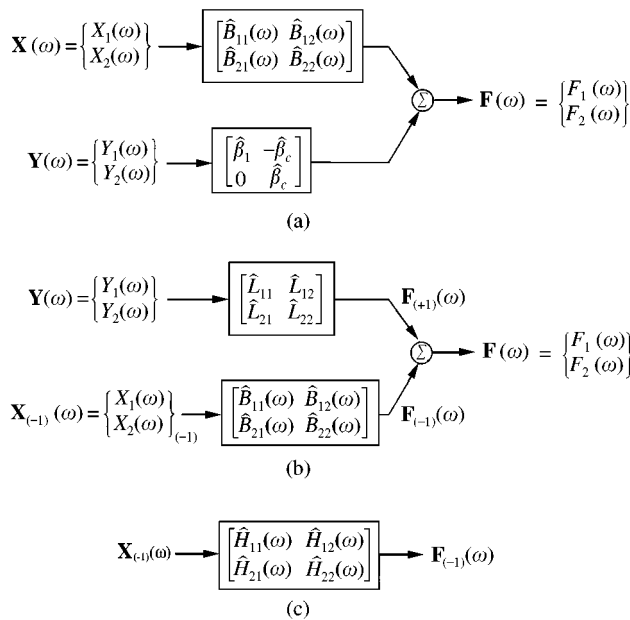
Figure 7. MIMO "reverse path" spectral model of example system derived from Method B. (a) Model with correlated inputs, equation (13). (b) Conditioned model with uncorrelated inputs. (c) "Forward path" of the underlying linear system.
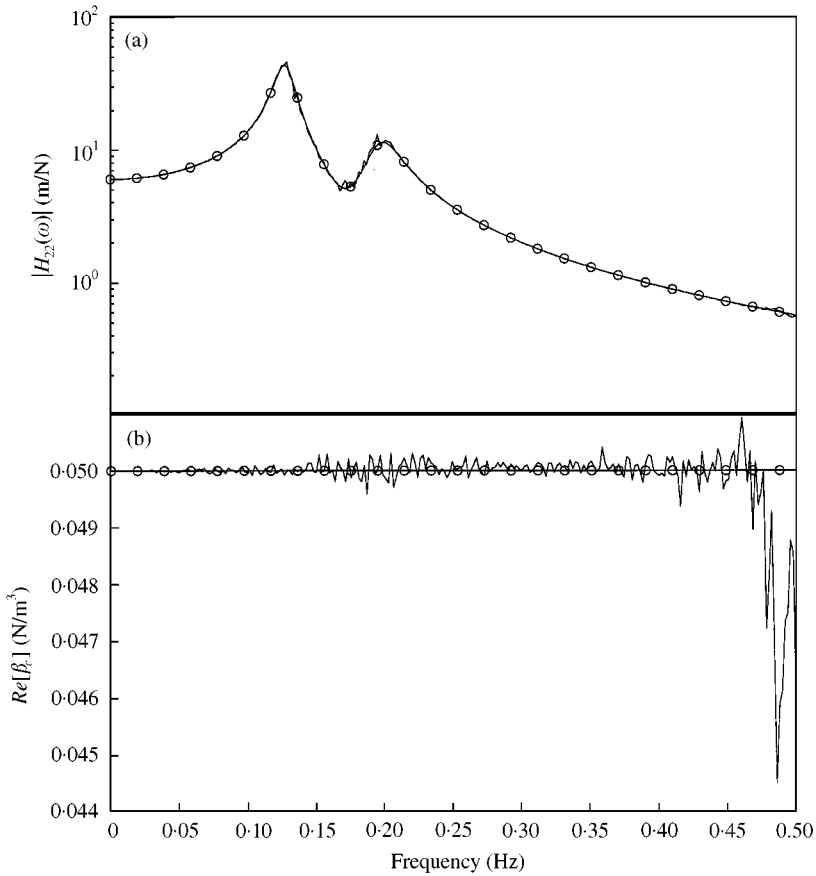
Figure 8. Multi-excitation results of Method B. (a) m.d.o.f. compliance function $H_{22}(\omega)$: ——, $|\hat{H}_{22}^{[c2]}(\omega)|$; –O–O–, $|H_{22}(\omega)|$. (b) Real part of coefficient β_c: ——, $\text{Re}[\hat{\beta}_c]$; –O–O–, β_c.

identification [12], natural frequencies, damping ratios and mode shapes can be determined. Since the conditioned dynamic compliance spectra are accurate estimates of the underlying linear system's dynamic compliance functions, as the sample result shows in Figure 8(a), these modal parameters will be accurate estimates of the underlying linear system's modal parameters.

Once the dynamic compliance functions have been determined, the coefficient matrix $\hat{\mathbf{a}}_1$ is estimated using equation (9). Explicitly for this example, the equation takes the following form:

$$\hat{\mathbf{a}}_1^{\text{T}}\hat{\mathbf{H}}^{\text{T}}(\omega) = \mathbf{G}_{11}^{-1}(\omega)(\mathbf{G}_{1F}(\omega)\hat{\mathbf{H}}^{\text{T}}(\omega) - \mathbf{G}_{1X}(\omega)),$$

$$\begin{bmatrix} \hat{\beta}_1 & 0 \\ -\hat{\beta}_c & \hat{\beta}_c \end{bmatrix}\begin{bmatrix} \hat{H}_{11}(\omega) & \hat{H}_{21}(\omega) \\ \hat{H}_{12}(\omega) & \hat{H}_{22}(\omega) \end{bmatrix}$$

$$= \begin{bmatrix} G_{11}(\omega) & G_{12}(\omega) \\ G_{21}(\omega) & G_{22}(\omega) \end{bmatrix}^{-1}\left(\begin{bmatrix} G_{1F_1}(\omega) & G_{1F_2}(\omega) \\ G_{2F_1}(\omega) & G_{2F_2}(\omega) \end{bmatrix}\begin{bmatrix} \hat{H}_{11}(\omega) & \hat{H}_{21}(\omega) \\ \hat{H}_{12}(\omega) & \hat{H}_{22}(\omega) \end{bmatrix} - \begin{bmatrix} G_{1X_1}(\omega) & G_{1X_2}(\omega) \\ G_{2X_1}(\omega) & G_{2X_2}(\omega) \end{bmatrix}\right).$$

$$(14a, b)$$
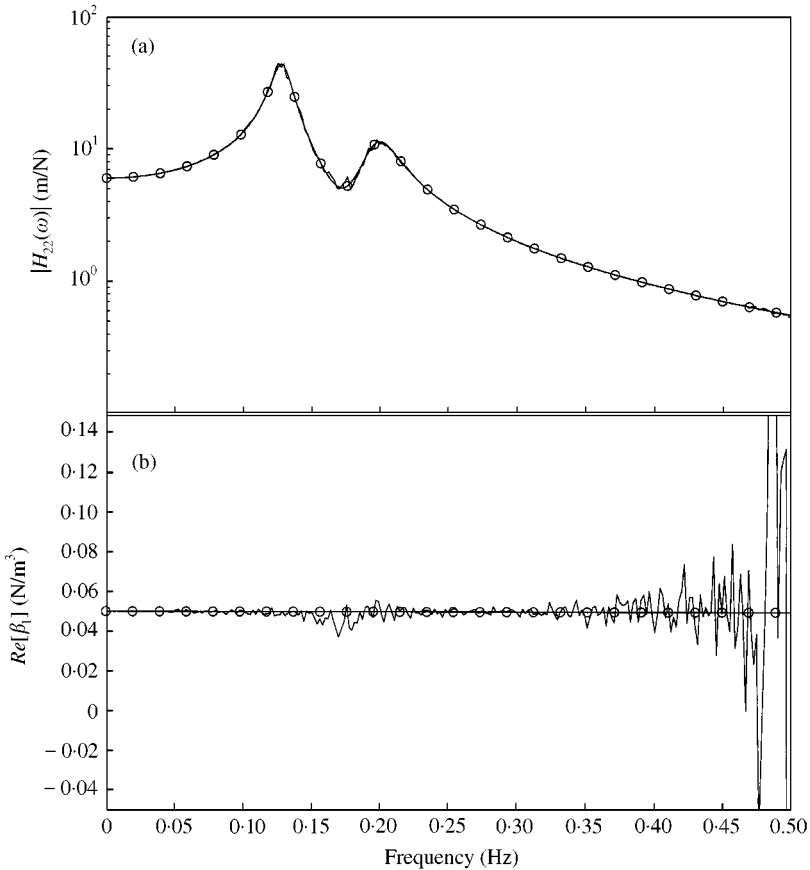
Figure 9. Single excitation results of Method B. (a) m.d.o.f compliance function $H_{22}(\omega)$: ——, $|\hat{H}_{22}^{[c2]}(\omega)|$; –O–O–, $|H_{22}(\omega)|$. (b) Real part of coefficient β_1: ——, $\mathrm{Re}[\hat{\beta}_1]$; –O–O–, β_1.

Here, since excitations have been applied to both m_1 and m_2, then $\hat{\mathbf{H}}^{\mathrm{T}}(\omega)$ is fully populated. Therefore, $[\hat{\mathbf{H}}^{\mathrm{T}}(\omega)]^{-1}$ can be post-multiplied to both sides of equation 14(b) in order to obtain estimate $\hat{\beta}_1$ and $\hat{\beta}_c$. The spectrum $\mathrm{Re}[\hat{\beta}_c]$ is illustrated in Figure 8(b) along with the actual value of β_c. As illustrated, the spectrum accurately estimates the real value β_c. Although $\mathrm{Im}[\hat{\beta}_c]$ is not shown, the spectrum is approximately equal to zero. For $\hat{\beta}_1$, the results are similar, $\mathrm{Re}[\hat{\beta}_1] \approx \beta_1$, $\mathrm{Im}[\hat{\beta}_1] \approx 0$.

Now consider the case where excitation is only applied to m_2. Since $F_1(\omega) = 0$, only the second column of the dynamic compliance matrix $\hat{\mathbf{H}}(\omega)$ can be determined,

$$\hat{\mathbf{H}}(\omega) = \begin{bmatrix} ? & \hat{H}_{12}(\omega) \\ ? & \hat{H}_{22}(\omega) \end{bmatrix}, \tag{15}$$

where ? indicates the unknown dynamic compliance functions that cannot be estimated from the single excitation data. The compliance $\hat{H}_{22}^{[c2]}(\omega)$ is shown in Figure 9(a) illustrating that the underlying linear system compliance $H_{22}(\omega)$ is accurately estimated. Notice that this is the same compliance function shown in Figure 8(a) for the multiple excitation case and that an equal amount of accuracy is obtained for both multiple and single excitations. Although only the second column of $\hat{\mathbf{H}}(\omega)$ is determined, modal parameter estimation

techniques [12] can still be applied to the two known estimates of equation (15) in order to obtain the systems underlying modal parameters unaffected by the non-linearities. Now since $\hat{\mathbf{H}}(\omega)$ is the underlying linear dynamic compliance matrix, reciprocity is valid and can be applied to determine $\hat{H}^r_{21}(\omega) = \hat{H}_{12}(\omega)$, where superscript r signifies that the function has been determined from reciprocity. Using this additional element in equation (15) and plugging equation (15) into equation (14a) gives

$$
\begin{bmatrix} \hat{\beta}_1 & 0 \\ -\hat{\beta}_c & \hat{\beta}_c \end{bmatrix}\begin{bmatrix} ? & \hat{H}^r_{21}(\omega) \\ \hat{H}_{12}(\omega) & \hat{H}_{22}(\omega) \end{bmatrix}
$$
$$
= \begin{bmatrix} G_{11}(\omega) & G_{12}(\omega) \\ G_{21}(\omega) & G_{22}(\omega) \end{bmatrix}^{-1}\left(\begin{bmatrix} 0 & G_{1F_2}(\omega) \\ 0 & G_{2F_2}(\omega) \end{bmatrix}\begin{bmatrix} ? & \hat{H}^r_{21}(\omega) \\ \hat{H}_{12}(\omega) & \hat{H}_{22}(\omega) \end{bmatrix} - \begin{bmatrix} G_{1X_1}(\omega) & G_{1X_2}(\omega) \\ G_{2X_1}(\omega) & G_{2X_2}(\omega) \end{bmatrix}\right). \quad (16)
$$

Notice, since $F_1(\omega) = 0$, the first column of $\mathbf{G}_{1F}(\omega)$ contains zeros. By multiplying out the left-hand side of equation (16), the significance of reciprocity can be seen,

$$
\begin{bmatrix} ? & \hat{\beta}_1 \hat{H}^r_{21}(\omega) \\ ? & \hat{\beta}_c(\hat{H}_{22}(\omega) - \hat{H}^r_{21}(\omega)) \end{bmatrix}
$$
$$
= \begin{bmatrix} G_{11}(\omega) & G_{12}(\omega) \\ G_{21}(\omega) & G_{22}(\omega) \end{bmatrix}^{-1}\left(\begin{bmatrix} 0 & G_{1F_2}(\omega) \\ 0 & G_{2F_2}(\omega) \end{bmatrix}\begin{bmatrix} ? & \hat{H}^r_{21}(\omega) \\ \hat{H}_{12}(\omega) & \hat{H}_{22}(\omega) \end{bmatrix} - \begin{bmatrix} G_{1X_1}(\omega) & G_{1X_2}(\omega) \\ G_{2X_1}(\omega) & G_{2X_2}(\omega) \end{bmatrix}\right). \quad (17)
$$

Using the equations from the second column of equation (17), $\hat{\beta}_1$ and $\hat{\beta}_c$ can be determined. Notice, without the use of reciprocity, $\hat{\beta}_1$ and $\hat{\beta}_c$ cannot be determined. As shown in Figure 9(b), the spectrum of $\hat{\beta}_1$ is an accurate estimate of β_1. Although not shown, the spectrum of $\hat{\beta}_c$ is also an accurate estimate of β_c. Now, a complete system model has been identified with excitation only applied to m_2.

8. CONCLUSION

The mathematical steps and the illustrative example described in this paper highlight two unique identification procedures for non-linear systems. Method A [11] identifies individual "reverse path" models for each of the equations of motion describing the non-linear system. From each model, physical properties of the underlying linear system can be determined using s.d.o.f. identification techniques [14]. However, in order to identify the entire system utilizing Method A, excitations are necessary at every response location. Method B [9] overcomes this limitation by identifying one "reverse path" model that includes all of the equations of motion. Modal parameters of the underlying linear system are then extracted from m.d.o.f. frequency response functions using m.d.o.f. modal parameter estimation techniques [12]. This establishes the core difference between the two methods discussed in this paper. Arguably, Method A is advantageous since physical properties are identified, and typically physical domain properties are preferred over modal domain properties (modal properties can be determined from physical properties but the opposite is not always true). However, since excitations must be applied and measured at each response location for complete identification of the system, application of Method A to systems with a large number of d.o.f.s could be a difficult task. Although Method B obtains model parameters of the underlying linear system, the advantage of the method is that it is better suited for systems with a large number of d.o.f.s where it may not be feasible to apply

excitations to each response location. Future work is encouraged in this area including application of both methods to real-life experiments.

REFERENCES

1. H. J. RICE and J. A. FITZPATRICK 1988 *Mechanical Systems & Signal Processing* **2**, 195–207. A generalized method for spectral analysis of non-linear system.
2. H. J. RICE and J. A. FITZPATRICK 1991 *ASME, Journal of Vibration and Acoustics* **113**, 132–140. The measurement of non-linear damping in single degree-of-freedom systems.
3. H. ESMONDE, J. A. FITZPATRICK, H. J. RICE and F. AXISA 1992 *Journal of Fluids and Structures* **6**, 223–248. Modeling and identification of non-linear squeeze film dynamics.
4. H. ESMONDE, J. A. FITZPATRICK, H. J. RICE and F. AXISA 1992 *Proceedings of the Institution of Mechanical Engineers* **206**, 225–238. Reduced order modeling of non-linear squeeze film dynamics.
5. J. S. BENDAT 1990 *Nonlinear System Analysis and Identification from Random Data.* New York: John Wiley & Sons, Inc.
6. J. S. BENDAT, P. A. PALO and R. N. COPPOLINO 1992 *Probabilistic Engineering Mechanics* **7**, 43–61. A general identification technique for nonlinear differential equations of motion.
7. J. S. BENDAT 1993 *Shock and Vibration* **1**, 21–31. Spectral techniques for nonlinear system analysis and identification.
8. J. S. BENDAT, R. N. COPPOLINO and P. A. PALO 1995 *International Journal of Non-Linear Mechanics* **30**, 841–860. Identification of physical parameters with memory in non-linear systems.
9. C. M. RICHARDS and R. SINGH 1998 *Journal of Sound and Vibration* **213**, 673–708. Identification of multi-degree-of-freedom nonlinear systems under random excitations by the "reverse path" spectral method.
10. C. M. RICHARDS and R. SINGH 1999 *Journal of Sound and Vibration* **220**, 413–450. Feasibility of identifying non-linear vibratory systems consisting of unknown polynomial forms.
11. H. J. RICE and J. A. FITZPATRICK 1991 *Journal of Sound and Vibration* **149**, 397–411. A procedure for the identification of linear and non-linear multi-degree-of-freedom systems.
12. R. J. ALLEMANG and D. L. BROWN 1998 *Journal of Sound and Vibration* **211**, 301–322. A unified matrix polynomial approach to modal identification.
13. J. S. BENDAT and A. G. PIERSOL 1986 *Random Data*: *Analysis and Measurement Procedures.* New York: Wiley-Interscience, second edition.
14. D. J. EWINS 1986 *Modal Testing*: *Theory and Practice.* Letchworth, Hertfordshire, England: New York: Research Studies Press; Wiley.
15. G. F. FORSYTHE, M. A. MALCOLM and C. B. MOLER 1977 *Computer Methods for Mathematical Computations.* Englewood Cliffs, NJ: Prentice-Hall.
16. L. D. MITCHELL 1982 *American Society of Mechanical Engineers, Journal of Mechanical Design* **104**, 277–279. Improved methods for the fast fourier transform (FFT) calculation of the frequency response function.